CrossMark

Improved Digital Rational Approximation of the Operator S^α Using Second-Order s-to-z Transform and Signal Modeling

Fouzia Leulmi · Youcef Ferdi

Abstract In this paper, an improved stable digital rational approximation of the fractional-order operator $s^\alpha, \alpha \in R$ is developed. First, a novel efficient second-order digital differentiator is derived from the transfer function of the digital integrator proposed by Tseng. Then, the fractional power of the new s-to-z transform is expanded using power series expansion (PSE)-signal-modeling technique to obtain stable rational approximation of s^α. Simulation results show that the proposed rational approximation has better frequency characteristics in almost the whole frequency range than that of existing first-order s-to-z transforms based approximations for different values of the fractional-order α. This paper also shows the benefit of using PSE-signal-modeling approach with first- or second-order mapping functions over PSE-truncation approach that is used in recent works for rational approximation of the operator s^α, and highlights the major disadvantage of the latter approach that leads to undesirable rational models with complex conjugate poles and zeros.

1 Introduction

The fractional-order derivative and integral of order α of an analog signal $x_a(t)$ are often denoted by the operator $_cD_t^\alpha x_a(t)$, where c and t are the lower and upper limits,

F. Leulmi (✉) · Y. Ferdi
LRES Laboratory, Electrical Engineering Department, Skikda University, BP. 26, Route d'El-Hadaîek,
21000 Skikda, Algeria
e-mail: leulmif@yahoo.fr

Y. Ferdi
e-mail: yferdi@yahoo.fr

Birkhäuser

respectively. The fractional operator $_c D_t^\alpha x_a(t)$ appears naturally in fractional order differential equations that best model many systems in various areas of engineering and sciences [4,17,27]. Upon zero initial conditions, fractional-order operators are represented by the transfer function

$$H_\alpha(s) = s^\alpha. \tag{1}$$

In the present study, the order α is assumed to be a real number, the lower limit c to be zero, and the fractional-order operator is simply denoted by the operator D^α.

The case $\alpha > 0$ indicates fractional-order differentiation, while the case $\alpha < 0$ indicates fractional-order integration. Fractional-order differentiation/integration-based algorithms have been used to solve many problems in various fields including automatic control [5,18,22,24], digital signal processing [3,11,12,20,21,23], and circuit theory and design [15,26]. The main problem encountered when dealing with fractional-order operator is how to realize it physically. This problem is due to the fact that fractional-order operators possess an infinite memory. Therefore, for physical implementation, approximate models with finite memory such Moving Average (MA), Autoregressive (AR), or Autoregressive Moving Average (ARMA) models are to be used instead. Although many methods have been developed to achieve such approximations with analog or digital models, this important issue in fractional-order calculus applications still needs to be addressed through new approaches that seem to be more promising in terms of approximation accuracy and computational complexity. In this paper, we focus on digital design case. The digital design methods of fractional-order integrator and differentiator can generally be classified into two categories: direct and indirect methods. In indirect methods [6,16,33], a rational continuous time model approximation of s^α is first developed, then the resulting s-transfer function is discretized using an appropriate s-to-z transform, whereas the direct methods substitute for s in s^α a chosen s-to-z transform, then the resulting non-rational z-transfer functions are approximated with rational ones. In the early direct discretization methods, the first-order s-to-z transforms of Euler, Tustin, and the linear combination of two of them (Al-Alaoui operator), have been used for discretization of s^α. In [7], the authors have proposed two discretization methods of s^α, i.e., a recursive discretization of Tustin operator and direct discretization using Al-Alaoui operator via continuous fraction expansion (CFE)-truncation. In [8] a family of second-order mapping functions obtained by inverting and stabilizing the combination of the numerical integrator rules of trapezoidal and Simpson have been used with CFE to design rational approximation of s^α. The design of finite impulse response (FIR) and infinite impulse response (IIR) fractional-order Simpson integrators using power series expansion (PSE)-truncation approach is proposed in [29].

More recently, higher order s-to-z transforms have been proposed for digital design of s^α in the hope of improving their approximation accuracy. In [14,30], the authors have proposed the use of higher order s-to-z transforms viz. second-order Schneider operator, and stabilized third-order Al-Alaoui-Schneider-Kaneshige-Groutage (Al-Alaoui-SKG) rule. The obtained approximations have been designed using PSE-truncation approach and compared with Al-Alaoui (CFE)-based approximations. These higher order s-to-z transforms have been modified in [32] to improve

the approximations in the low frequencies. However, simulation results showed that the Schneider operator and Al-Alaoui-SKG (PSE-truncation) based approximations possess complex conjugate poles and zeros which may be not desirable since it is well known that, for a better fit to continuous frequency response of s^α, it would be of high interest to obtain discrete approximation with poles and zeros distributed in alternating fashion on the real axis in the unit circle in the z plane [25,31].

The signal-modeling approach proposed in [9,10,13] has proved to be an efficient method for digital rational design of s^α. Indeed, it is computationally efficient and leads to rational approximations with the desired properties, namely, stability, minimum phase and poles- zeros distributed in alternating fashion on the real axis. The contribution of the present study is to improve the rational approximation of s^α obtained via PSE-signal-modeling approach by using a new second-order s-to-z transform (new mapping function (NMF)) [19]. This s-to-z transform has been derived through inversion and stabilizing of the transfer function of the digital integrator designed using conventional Simpson-integrator rule and fractional delay filter proposed by Tseng in [28]. As it will be shown in the sequel, compared to the magnitude response of the ideal integrator $1/s$, the magnitude response of the integrator proposed by Tseng outperforms the integrators corresponding to the first and higher order s-to-z transforms mentioned above.

Simulation results show that the proposed rational approximation of s^α has better frequency characteristics (magnitude and phase responses) than those based on the widely used Al-Alaoui operator and Euler's rule, in a wide range of frequencies. It has also better magnitude frequency response than that of Al-Alaoui-Schneider, Hsue operator [14], and Tustin based approximations. The latter, however, has the best phase response.

Furthermore, this paper compares the NMF (PSE-signal modeling)-based approximations to those obtained using PSE-truncation approach used in [14,29,30]. The simulation results confirm that the major disadvantage of PSE-truncation approach for rational approximation of s^α is that it provides models having complex conjugate poles and zeros.

The rest of the paper is organized as follows: In Sect. 2, after a brief introduction of the integer order digital integrator proposed by Tseng in [28], the corresponding new stabilized digital differentiator is presented. Section 3 derives the impulse response of the new digital fractional-order differentiator (NDFOD). Simulation results are presented in Sect. 4, and the impulse response derived in Sect. 3 has been modeled to calculate the IIR models which have been compared to those obtained based on recently used s-to-z transforms. In Sect. 4, we have compared the approximations obtained using PSE-signal modeling with those obtained using PSE-truncation approach. Conclusions are provided in Sect. 5.

2 Novel Stable Second-Order s-to-z Transform

The novel stable second-order s-to-z transform introduced in this paper is obtained by inverting and stabilizing the second-order digital integrator designed from the conventional Simpson integrator and fractional delay filter proposed by Tseng in [28].

2.1 Digital Integrator Proposed by Tseng

In [28], Tseng has proposed a new non-minimum phase integrator in order to improve the magnitude response of the conventional Simpson integrator by reducing the sampling interval from T to $0.5T$. The whole process can be summarized as follows:

Firstly, replacing T by $0.5T$ in the expression of the output $y(n)$ of the conventional Simpson integrator and taking the z transform yield the following z transfer function [28]

$$G(z) = \frac{T(1 + 4z^{-1/2} + z^{-1})}{6(1 - z^{-1})} \tag{2}$$

The fractional delay element $z^{-1/2}$ is then implemented with IIR all-pass filter and FIR filter using the design technique of FIR and all-pass fractional delay filter [28].

In this paper, the designed digital integrator obtained by using the following half sample delay IIR all-pass filter [28] is investigated

$$z^{-1/2} = \left(1/3 + z^{-1}\right) \Big/ \left(1 + (1/3)z^{-1}\right) \tag{3}$$

Substituting (3) in (2), we obtain the transfer function derived in [28]

$$G(z) = \frac{T}{6} \frac{7 + 16z^{-1} + z^{-2}}{3 - 2z^{-1} - z^{-2}} \tag{4}$$

The integrator in (4) has two real zeros located at $z = -2.2214$, and $z = -0.064309$, and two poles at $z = 1$ and $z = -0.333333$. To illustrate the performance of the integrator in (4), Fig. 1 shows the percent relative error in magnitude defined in (5) between the ideal integrator $1/s$ and the integrators corresponding to the first and higher order s-to-z transforms [1] listed in Table 1.

$$Er = \left(|Hi| - \left|H_{app}\right|\right)/|Hi| \quad (\%), \tag{5}$$

where $H_{i=} s^{-1}\big|_{s=j2\pi f}$, and $H_{app} = [M(z)]^{-1}\big|_{z=e^{j2\pi fT}}$ with $M(z)$ represents the s-to-z transforms.

We can observe from this figure that the integrator in (4) presents the smallest error over almost the whole frequency range, especially at high frequencies where it overlaps the Al-Alaoui-SKG curve.

2.2 New Stable Digital Differentiator

The direct inversion of the transfer function $G(z)$ in (4) leads to instable recursive differentiator since $G(z)$ is non-minimum phase as one zero ($z = -2.2214$) lies outside the unit circle in the z plane.

Let $H(z)$ be the transfer function defined by

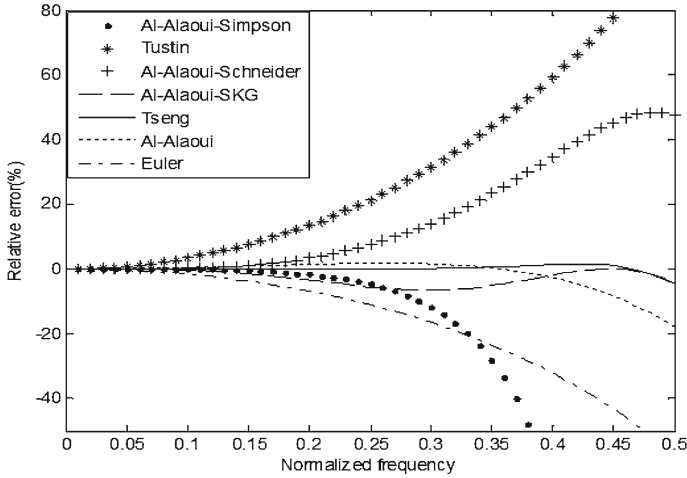$$H(z) = \frac{1}{G(z)} = \frac{6}{T} \frac{3 - 2z^{-1} - z^{-2}}{7 + 16z^{-1} + z^{-2}} \tag{6}$$

Fig. 1 Percent relative error of integrators, $T = 1$s

Table 1 s-to-z transforms

Method	Conversion s-to-z
Euler	$s \approx \frac{1-z^{-1}}{T}$
Tustin	$s \approx \frac{2}{T}\frac{1-z^{-1}}{1+z^{-1}}$
Al-Alaoui	$s \approx \frac{8}{7T}\frac{1-z^{-1}}{1+z^{-1}/7}$
Al-Alaoui-Simpson	$s \approx \frac{0.8038475773}{T}\frac{(1-z^{-2})}{(1+0.2679491924Z^{-1})^2}$
Al-Alaoui-SKG	$s \approx \frac{1.1272}{T}\frac{(z^3-z^2)}{(z^3+0.168z^2-0.0607z+0.0199)}$
Al-Alaoui-Schneider	$s \approx \frac{1.398181667894}{T}\frac{(1-z^{-1})}{(1+0.4660655596Z^{-1}-0.067878888z^{-2})}$

This may be written in factorizing form as

$$H(z) = \frac{1}{G(z)} = \left(\frac{18}{7T}\right)\frac{(1-z_1 z^{-1})(1-z_2 z^{-1})}{(1-p_1 z^{-1})(1-p_2 z^{-1})} \tag{7}$$

with $z_1 = 1$ and $z_2 = -0.333333$, $p_1 = -2.2214$ and $p_2 = -0.064309$. Notice that p_1 is an instable pole. Thus applying the pole reflection method used in [1,2], by inverting p_1 from radius $r = 2.2214$ to radius $1/r$ and compensating the resulting change in magnitude, we obtain the following new stable digital differentiator.

$$s \approx H(z) = \left(\frac{18}{7T(-p_1)}\right)((1-z_1 z^{-1})(1-z_2 z^{-1})/((1-(1/p_1)z^{-1})(1-p_2 z^{-1}))) \tag{8}$$
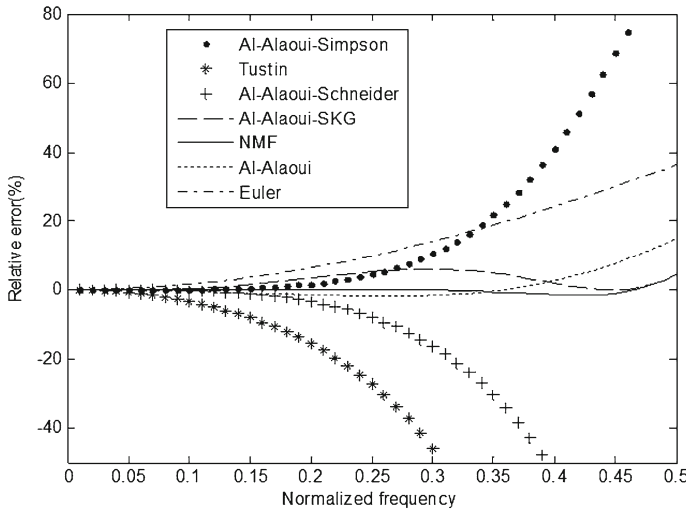
Fig. 2 Percent relative error of differentiators, $T = 1$s

To illustrate the performance of the new stable digital differentiator (NMF) in (8), Fig. 2 shows the percent relative error in magnitude between the ideal differentiator s and the new stable differentiator in (8) and the s-to-z transforms listed in Table 1.

We can observe from Fig. 2 that the NMF in (8) presents the smallest relative error over almost the whole frequency range. Indeed, the NMF approximates the ideal differentiator favorably, with $E_r \leq 2.91\,\%$.

The NDFOD is obtained by taking the $\alpha\,th$ power of the novel s-to-z transform given in (8) as follows:

$$s^\alpha \approx H^\alpha(z) = \left(\frac{18}{7T(-p_1)}\right)^\alpha \left(\left(1 - z_1 z^{-1}\right)^\alpha \right.$$

$$\left. \left(1 - z_2 z^{-1}\right)^\alpha \right) \Big/ \left(\left(1 - \frac{z^{-1}}{p_1}\right)^\alpha \left(1 - p_2 z^{-1}\right)^\alpha\right) \tag{9}$$

As can be seen, the expression in (9) is irrational function. The aim of this work is to transform it into rational transfer function (10), using PSE-signal-modeling technique, as follows:

$$F(z) = B(z)/A(z) = \left(\sum_{i=0}^{q} b_i z^{-i}\right) \Big/ \left(1 + \sum_{i=1}^{p} a_i z^{-i}\right) \tag{10}$$

The unknown coefficients a_i and b_i are to be determined such that the impulse response $h_F(n)$, the inverse z-transform of $F(z)$ in (10), best approximates the desired one $h_\alpha(n)$, the inverse z- transform of $H^\alpha(z)$ in (9), in some sense.

3 Derivation of the Impulse Response

In this section we derive the desired impulse response of the NDFOD. Rewriting first equation (9) in the factorizing form as

$$S^\alpha \approx \left(\frac{18}{7T(-p_1)}\right)^\alpha (1 - z_1 z^{-1})^\alpha (1 - z_2 z^{-1})^\alpha \left(1 - \frac{z^{-1}}{p_1}\right)^{-\alpha} (1 - p_2 z^{-1})^{-\alpha}$$

(11)

Denoting the four terms in (11) as follows

$$A_1(z) = (1 - z_1 z^{-1})^\alpha, \quad A_2(z) = (1 - z_2 z^{-1})^\alpha,$$

$$A_3(z) = \left(1 - \frac{z^{-1}}{p_1}\right)^{-\alpha}, \quad A_4(z) = (1 - p_2 z^{-1})^{-\alpha}$$

we can write

$$S^\alpha \approx \left(\frac{18}{7T(-p_1)}\right)^\alpha A_1(z) A_2(z) A_3(z) A_4(z)$$

(12)

By taking the PSE of each factor $A_i(z)$ in (12), we get

$$A_i(z) = \sum_{n=1}^{\infty} h_i(n) z^{-n} \qquad i = 1, 2, 3, 4$$

(13)

where $h_i(n)$ represent the inverse z-transforms of $A_i(z)$. The first L values of the desired impulse response, required for the computation of the rational approximation of $H^\alpha(z)$, can be computed via the discrete convolution of the first L values of $h_i(n)$, i =1,2,3,4, i.e.,

$$h(n) = h_1(n) * h_2(n) * h_3(n) * h_4(n) \quad and \quad h_\alpha(n) = \left(\frac{-18}{7Tp_1}\right)^\alpha h(n)$$

(14)

Once the desired impulse response has been computed, a signal modeling technique is then applied to estimate the coefficients a_i and b_i of the transfer function $F(z)$ approximating $H^\alpha(z)$. The degrees of the denominator and numerator polynomials p and q, respectively, are to be chosen by the designer. Many signal-modeling techniques such as Padé approximant, Prony, Shanks, or Steiglitz Mc-Bride methods can be used to estimate these coefficients. Simulation experiments showed that the Steiglitz–Mc Bride method can provide slight improvement in low frequencies as compared to non-iterative ones (Prony, Shanks). Therefore, in this paper, the coefficients a_i and b_i are obtained by modeling the impulse response $h_\alpha(n)$, using Steiglitz–Mc-Bride method. This method is implemented in Matlab by the function *stmcb.m*. Based on the above equations, the desired impulse response of the new digital half differentiator /integrator for $L = 500$, $T = 1s$ is plotted in Fig. 3. This impulse response will be modeled in the next section to calculate the coefficients of the rational approximation of NDFOD.
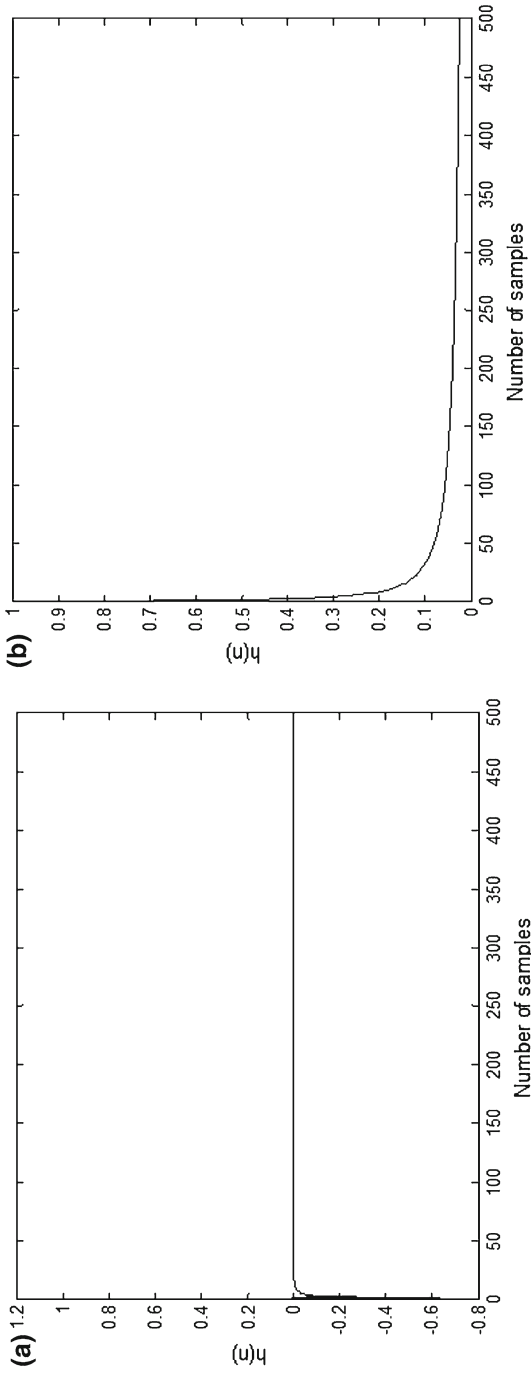
Fig. 3 Impulse response of the NDFOD, $L = 500$, $T = 1$ s, **a** $\alpha = 0.5$, **b** $\alpha = -0.5$

4 Simulation Results and Comparisons

4.1 Rational Approximation of s^α Using PSE-Signal modeling

In this section, we present simulation results for digital rational approximation (IIR filters) of continuous half differentiator $s^{0.5}$ and half integrator $s^{-0.5}$ sampled at $T = 1s$, for $p = q = 5$. The fifth-order models of half differentiator and half integrator based on NMF are obtained by modeling the impulse response presented in Fig. 3 using the Matlab's mfile stmcb.m. For comparison purposes, the Al-Alaoui, Tustin, Euler, Hsue, and Al-Alaoui-Schneider operators based rational models are designed using the same method. The coefficients a_i and b_i of the obtained rational approximations are reported in Table 2.

Figure 4 compares the magnitude and phase frequency responses of the rational approximations (in Table 2) with the ideal half differentiator $s^{0.5}$ and half integrator $s^{-0.5}$.

A zoomed view of the magnitude responses shows that the NMF improves the high frequency magnitude response comparatively to the Al-Alaoui Schneider, Al-Alaoui, Tustin, Euler, and Hsue operators. Also, the approximations based on NMF have better phase response than those based on the Al-Alaoui operator and Euler's rule in high frequency range and the phase is closer to the ideal one for larger range of frequencies using Tustin operator.

To see how well the magnitude frequency response is approximated in all the range of frequencies for half differentiator as well as half integrator, Fig. 5 shows the percent relative error in magnitude between the ideal continuous fractional-order operator s^α, $\alpha = \pm 0.5$ and the approximations defined by the coefficients given in Table 2.

We can observe from Fig. 5 that the NMF accomplishes better magnitude response fit with the smallest relative error which remains within about $Er = \pm 2.39\%$ for s^α, $\alpha = \pm 0.5$. In order to check for the stability of the obtained approximations, poles-zeros plots are shown in Fig. 6.

We can see that the poles and zeros are inside the unit circle in the z plane and distributed in alternating fashion that is the obtained rational approximations are stable and minimum phase. Considering now distinct order of differentiators and integrators, Figures 7 and 8 show the percent relative errors in magnitude of the rational approximations of s^α, for $\alpha = \pm 0.7$ and $\alpha = \pm 0.3$, respectively.

From the error plots, it can be observed that the differentiator and integrator of order $\alpha = 0.3$ and $\alpha = 0.7$ obtained by using NMF have the smallest error compared to those based on the others operators.

To further investigate the performance of the proposed approach, let us compare the existing third-order model of one-third integrator based on Hsue operator obtained using CFE, proposed in [14], with the third-order approximation obtained using NMF (PSE-signal modeling), suggested in this paper. From [14], the transfer function of the third-order model based on Hsue operator is given in (15), with $T = 0.001s$.

$$H_{\text{Hsue}-\text{cfe}-\frac{1}{3}} = 0.0794 \frac{(1 - 0.793z^{-1})(1 - 0.2646z^{-1})(1 + 0.1922z^{-1})}{(1 - 0.9108z^{-1})(1 - 0.4548z^{-1})(1 + 0.07365z^{-1})} \quad (15)$$

Table 2 Coefficients of the rational approximations $B(z)/A(z)$ using PSE-signal modeling

|			Al-Alaoui	Tustin	Euler	Hsue	NMF	Al-Alaoui-Schneider
$\alpha = 0.5$	$A(z)$	a_0	1.00000000000000	1.00000000000000	1.00000000000000	1.00000000000000	1.00000000000000	1.00000000000000
		a_1	−2.973314461443737	2.454743515965596	−3.274308265484677	−2.650216096776443	−2.261135485534702	−1.799083369771968
		a_2	3.135238561983327	1.396341702177269	3.986841822179217	2.296080031037996	1.375047151911086	0.491475908229836
		a_3	−1.320341978722998	−0.741906257411045	−2.168835542072618	−0.584905098095389	0.108674005707644	0.524323732893112
		a_4	0.140337393772762	−0.850001216683816	0.480403502365723	−0.093267368621682	−0.243360686831369	−0.205679902018916
		a_5	0.017786859124045	−0.166502211756375	−0.024064425527295	0.032517865196636	0.026296404199011	−0.009273331870039
	$B(z)$	b_0	1.069044967644567	1.414213562407956	0.99999999997338	1.41421356237131	1.075903617903637	1.182447321403465
		b_1	−3.789489561781301	2.058098518006636	−3.774308061446693	−4.653611252597135	−3.063160437722001	−2.994114273193286
		b_2	5.080791711801894	−0.782612419929090	5.498988892127345	5.611585710935621	2.860509001769126	2.267021171125117
		b_3	−3.129340761402043	−.1978265690333552	−3.815386073078392	−2.906275239067603	−0.713355967200739	−0.206597292562161
		b_4	0.831436092275494	−0.374724094288653	1.231670588532633	0.524979944094750	−0.254799152676429	−0.303847061435426
		b_5	−0.061940142505705	0.176597075819296	−0.140964432369537	0.009114645663682	0.099918936608043	0.055153700741286
$\alpha = -0.5$	$A(z)$	a_0	1.00000000000000	1.00000000000000	1.00000000000000	1.00000000000000	1.00000000000000	1.00000000000000
		a_1	−3.989538583002417	−2.454743515965238	−4.113921351550792	−3.860219440056017	−3.625977143593134	−3.464062127200338
		a_2	6.188802303030616	1.396341732176246	6.635560452000796	5.731492858374611	4.919986665723462	4.365471880804308
		a_3	−4.616775958720103	0.741906257411778	−5.214303574434008	−4.016111357488470	−2.976152223904406	−2.275401572174952
		a_4	1.625414439086853	−0.850001216683669	1.977700293890100	1.278815006513773	0.696599185686775	0.311110508744688
		a_5	−0.207079963233808	0.166502211756159	−0.285035733035575	−0.133976864858487	−0.014456086005641	0.062881848594983
	$B(z)$	b_0	0.935414346854115	0.737106781133865	1.000000005956899	0.707106778464103	0.929451285105201	0.845703635790409
		b_1	−3.197491561098655	−1.029049258841858	−3.614114878111442	−2.276830299724312	−2.821260984269699	−2.309646267015290
		b_2	4.039946691327612	−0.391306210037394	4.955345959672640	2.613521608106713	2.954907485360616	1.908066647153831
		b_3	−2.223837054682416	0.989132845098902	−3.132899000036449	−1.181803923841088	−1.098771885386473	−0.154654147103890
		b_4	0.442336257209251	−0.187362047085791	0.857327746518975	0.096654216450709	−0.025462500Ο0995666	−0.399543661070911
		b_5	0.003637680603063	−0.088298537918810	−0.065655655683893	0.041359178974839	0.061154030651057	0.110098044776455
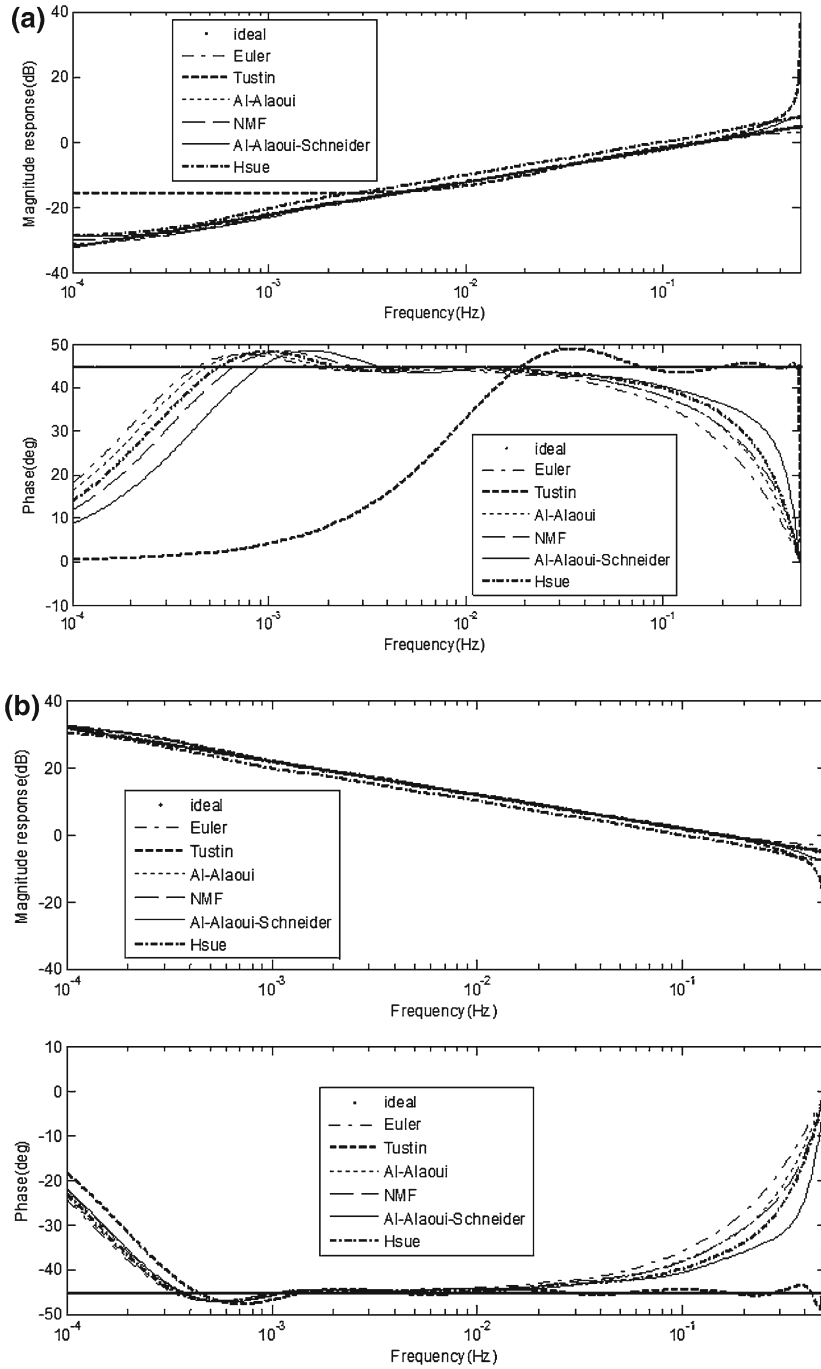
Fig. 4 Magnitude and phase responses of s^α and the corresponding approximations obtained using Steiglitz Mc-Bride based on first-order operators, Al-Alaoui-Schneider operator, and NMF **a** $\alpha = 0.5$, **b** $\alpha = -0.5$
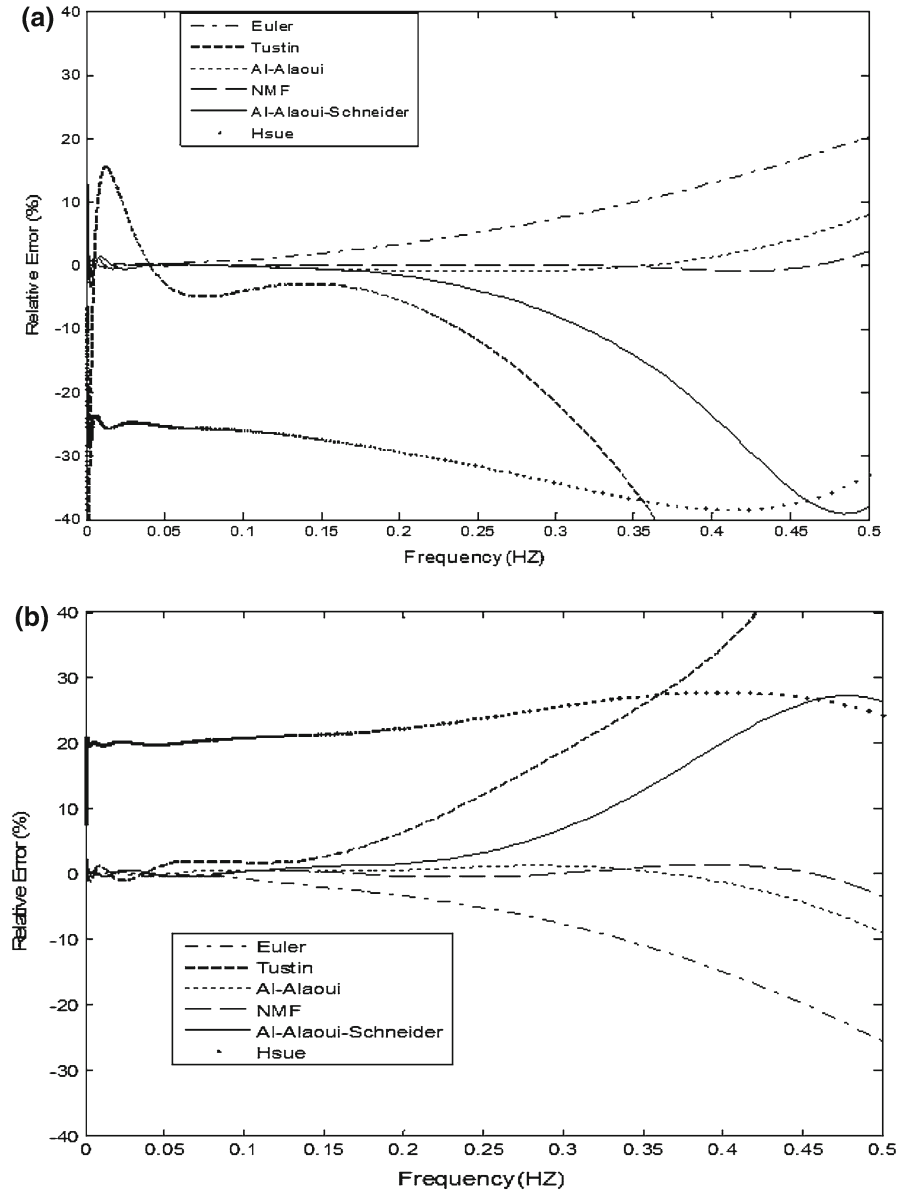
Fig. 5 Percent relative error corresponding to NMF, Al-Alaoui-Schneider, and first-order operators **a** $\alpha = 0.5$, **b** $\alpha = -0.5$

The transfer function of the third-order model of one-third integrator obtained using NMF (PSE-signal modeling) is given in equation (16).

$$H_{\text{NMF}-\text{PSE}-\text{signal modeling}-\frac{1}{3}} = \frac{0.0952 - 0.1964z^{-1} + 0.1174z^{-2} - 0.0161z^{-3}}{1 - 2.4474z^{-1} + 1.9240z^{-2} - 0.4766z^{-3}}$$
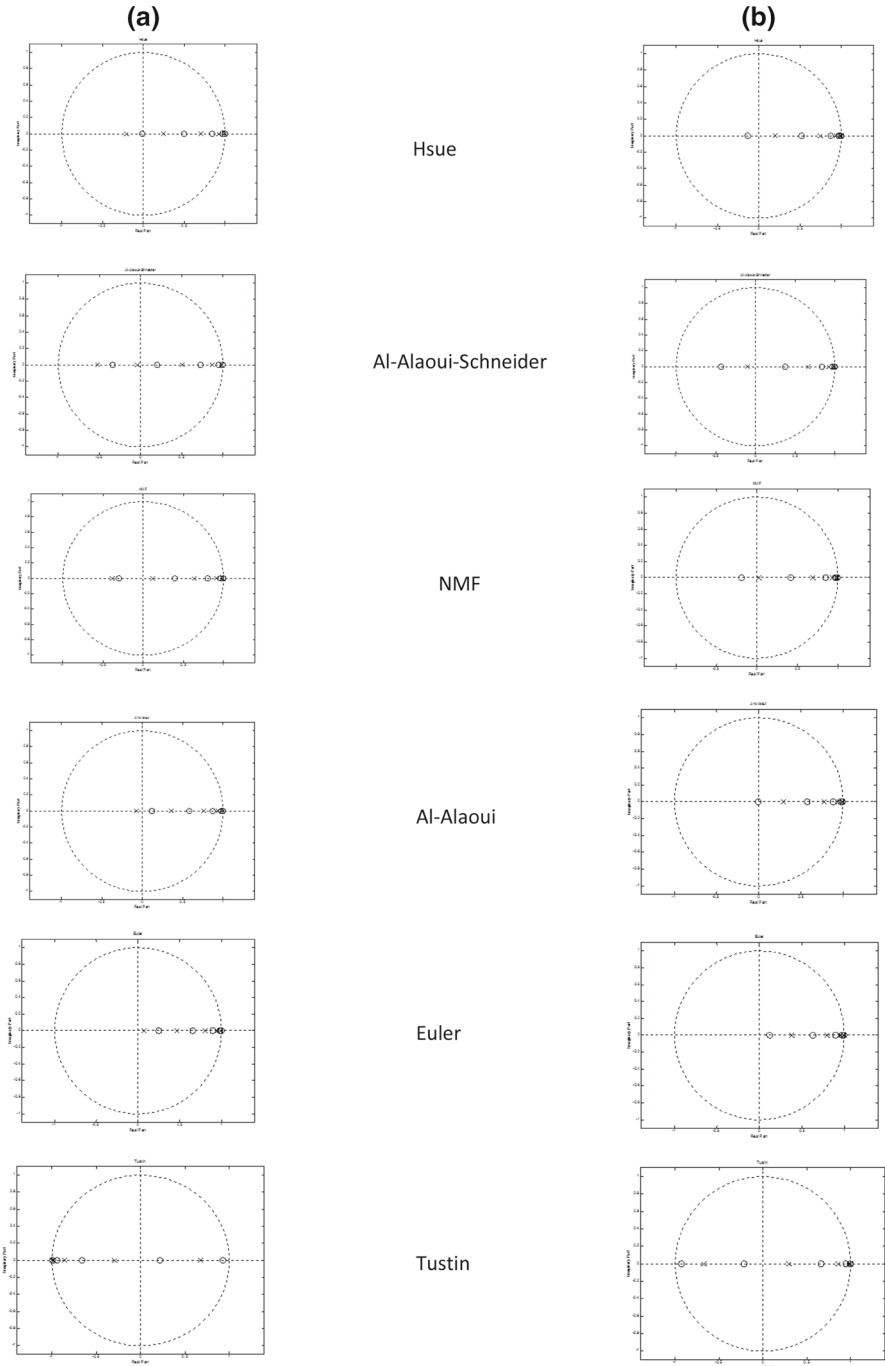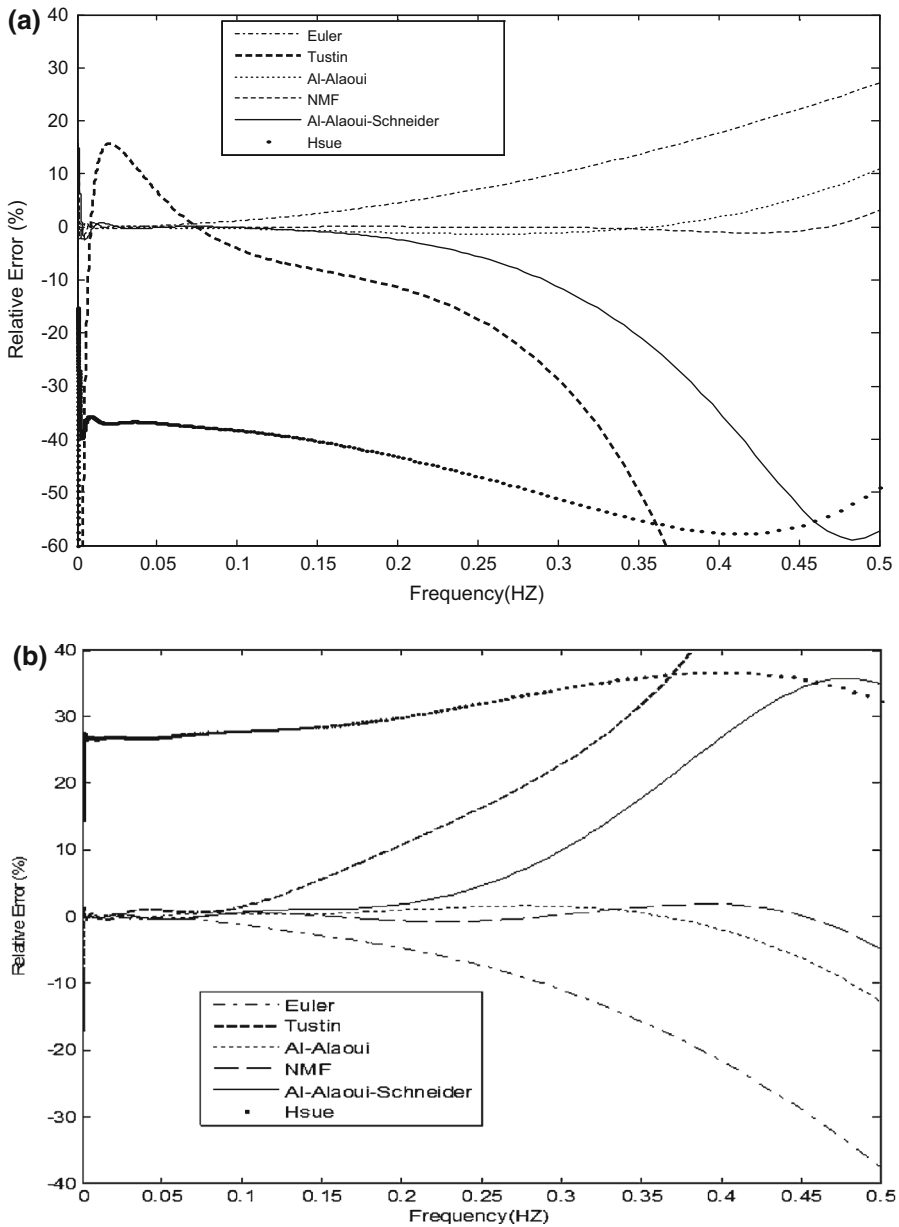
(16)

(a)   **(b)**

Hsue

Al-Alaoui-Schneider

NMF

Al-Alaoui

Euler

Tustin

Fig. 6 Poles-zeros diagram, **a** $\alpha = 0.5$, **b** $\alpha = -0.5$

Fig. 7 Percent relative error corresponding to NMF, Al-Alaoui-Schneider, and first-order operators **a** $\alpha = 0.7$, **b** $\alpha = -0.7$

The magnitude and phase responses corresponding to the transfer functions (15) and (16) along with that of the ideal continuous one-third integrator are presented in Fig. 9.
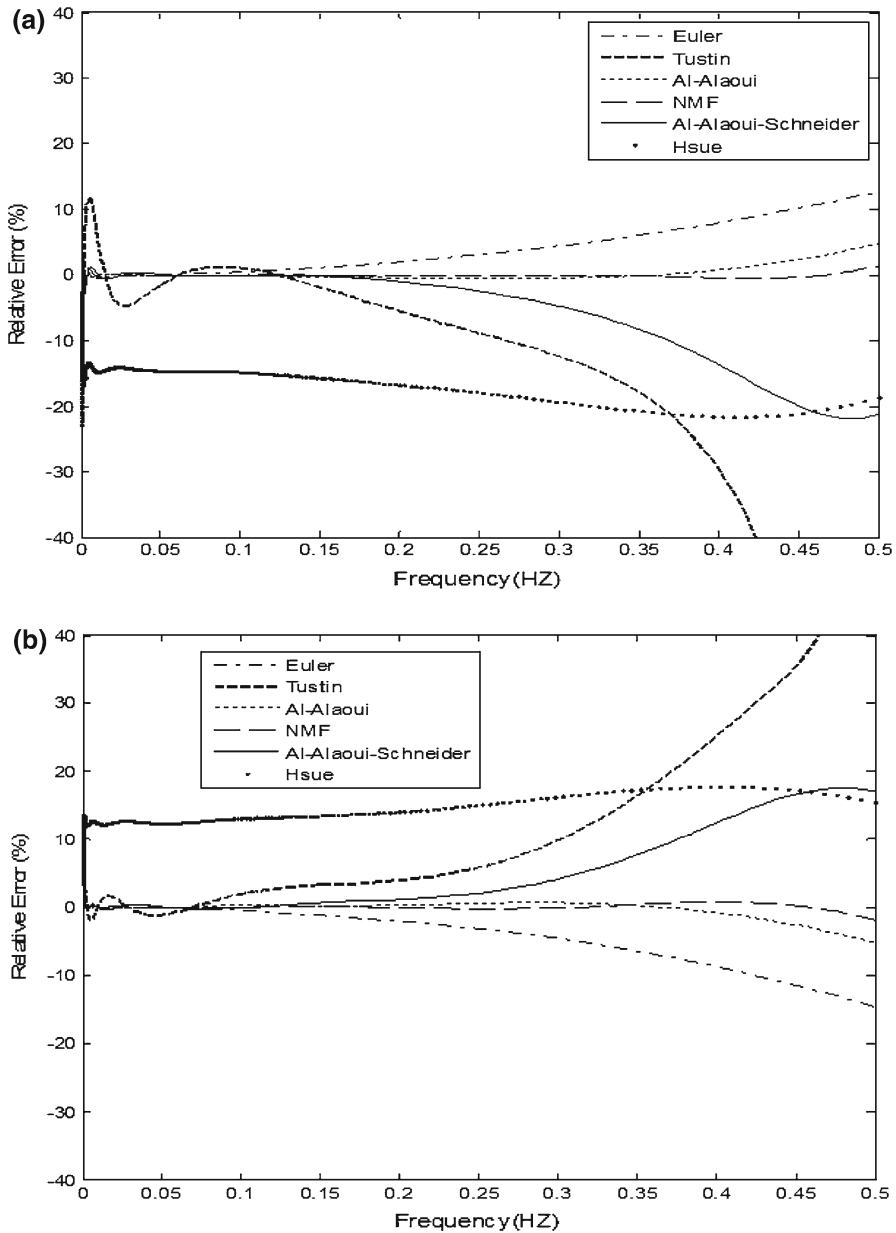
Fig. 8 Percent relative error corresponding to NMF, Al-Alaoui-Schneider, and first-order operators **a** $\alpha = 0.3$, **b** $\alpha = -0.3$

Figure 10 shows the percent relative error in magnitude between the ideal continuous one-third integrator and the approximations defined by eqs. (15) and (16). It is clear that the one-third integrator based on NMF has smaller approximation error than that of Hsue operator.
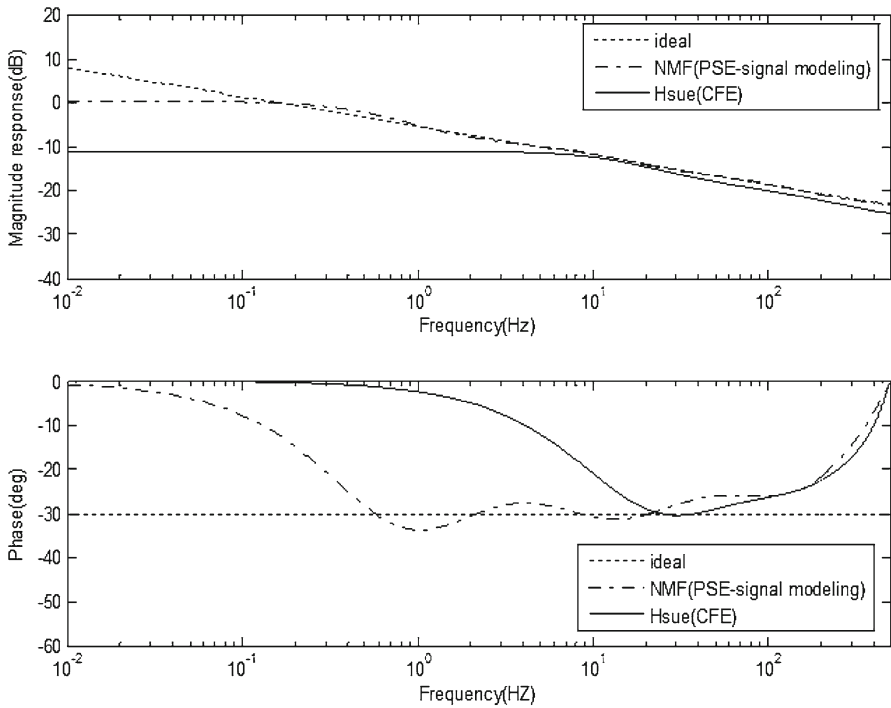
Fig. 9 Magnitude and phase responses of $s^{-1/3}$ and the approximations obtained using NMF (PSE-signal modeling) and Hsue (CFE), for $T = 0.001$s, $q = p = 3$
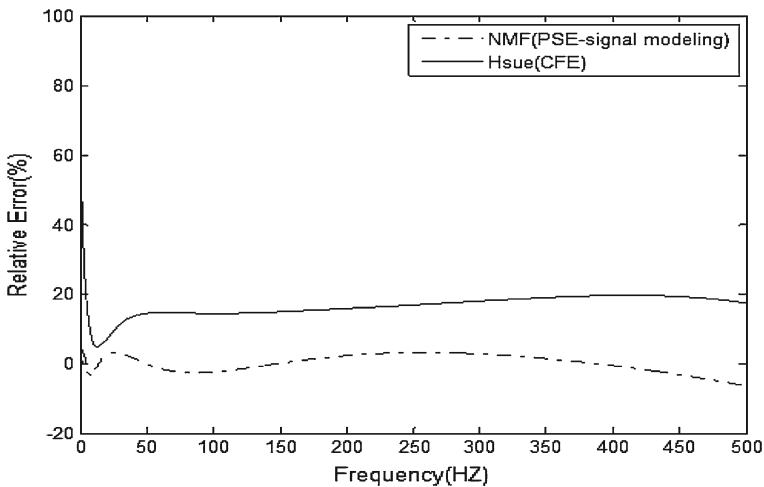

Fig. 10 Percent relative error corresponding to NMF (PSE-signal modeling) and Hsue (CFE)

Table 3 Coefficients of the rational approximations obtained using PSE- truncation and PSE-signal modeling based on NMF

		PSE-truncation		PSE-signal modeling	
		$\alpha = 1/4$	$\alpha = -1/4$	$\alpha = 1/4$	$\alpha = -1/4$
A(z)	a_0	1.000000000000000	1.000000000000000	1.000000000000000	1.000000000000000
	a_1	0.128618732779785	−0.128618732779785	−2.642298424462082	−3.346619696567223
	a_2	−0.017576702073245	0.034119480495123	2.180842137372684	4.053031823772161
	a_3	0.004654368244047	−0.011303465735543	−0.360042594479389	−2.015118863658326
	a_4	−0.001455440936101	0.004107625264022	−0.238434104364171	0.258795471839350
	a_5	0.000494219246776	−0.001567216047954	0.060014220570801	0.049913556402085
B(z)	b_0	1.037257739379952	0.964080538553298	1.037257739381558	0.964080538556493
	b_1	−0.172876289896659	0.160680089758883	−3.047027754055937	−2.941736892553446
	b_2	−0.129657217422494	0.147290082278976	2.999348950633721	3.105660127139822
	b_3	−0.060026489547451	0.100425056099302	−0.912125378920097	−1.173256118096685
	b_4	−0.043719293220393	0.085082339195242	−0.166892647491649	−0.020115601187619
	b_5	−0.031864061534772	0.071645838633807	0.089452730584446	0.065382467056951

4.2 PSE-signal Modeling Versus PSE-Truncation

In the rest of this section we will compare the performance of the PSE-signal modeling and PSE-truncation for rational approximation of s^α. An example is used for rational approximation of s^α, $\alpha = \pm 1/4$. Table 3 presents the coefficients of rational approximations of s^α, $\alpha = \pm 1/4$ obtained using PSE-signal modeling and PSE-truncation approaches based on NMF for $p = q = 5$, $T = 1s$, $L = 500$.

Figure 11 presents the magnitude and phase frequency responses of the rational approximations (in Table 3) along with that of the ideal fractional-order operator s^α, $\alpha = 1/4$ and $\alpha = -1/4$.

Figure 12 presents the percent relative error in magnitude, between the ideal continuous fractional-order operator s^α, $\alpha = \pm 1/4$ and the magnitude of the approximations obtained using PSE-signal modeling and PSE-truncation.

Figure 12 shows clearly that the error corresponding to PSE-signal modeling is smaller than that of the PSE-truncation. To check for the stability of the obtained approximations, Fig. 13 presents poles-zeros diagram of the approximations based on NMF.

We can deduce that PSE-signal modeling and PSE-truncation provide stable minimum phase filters since all poles and zeros are inside the unit circle. But unlike PSE-signal modeling, the PSE-truncation provides approximations which possess complex conjugate poles and zeros. The latter may not be desirable for approximation of s^α.

Now, let us compare the previous methods using the first-order Al-Alaoui operator. The rational models based on the Al-Alaoui operator using PSE-signal modeling and PSE-truncation for $\alpha = 0.5$, $p = q = 5$, $T = 1s$, $L = 500$ are defined by the coefficients given in Table 4.
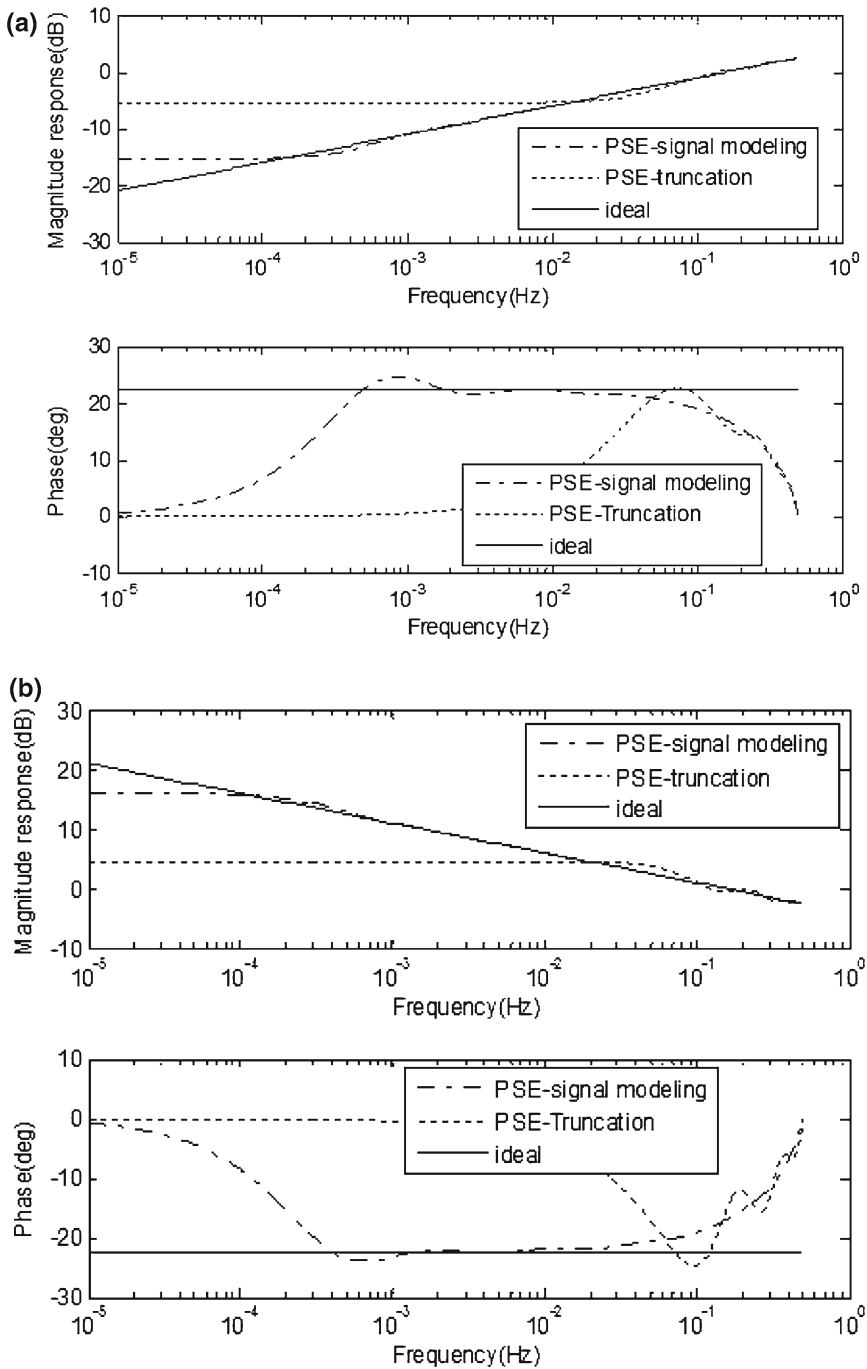
Fig. 11 Magnitude and phase responses of s^{α} and the approximations obtained using PSE-signal modeling and PSE-truncation based on NMF **a** $\alpha = 1/4$, **b** $\alpha = -1/4$
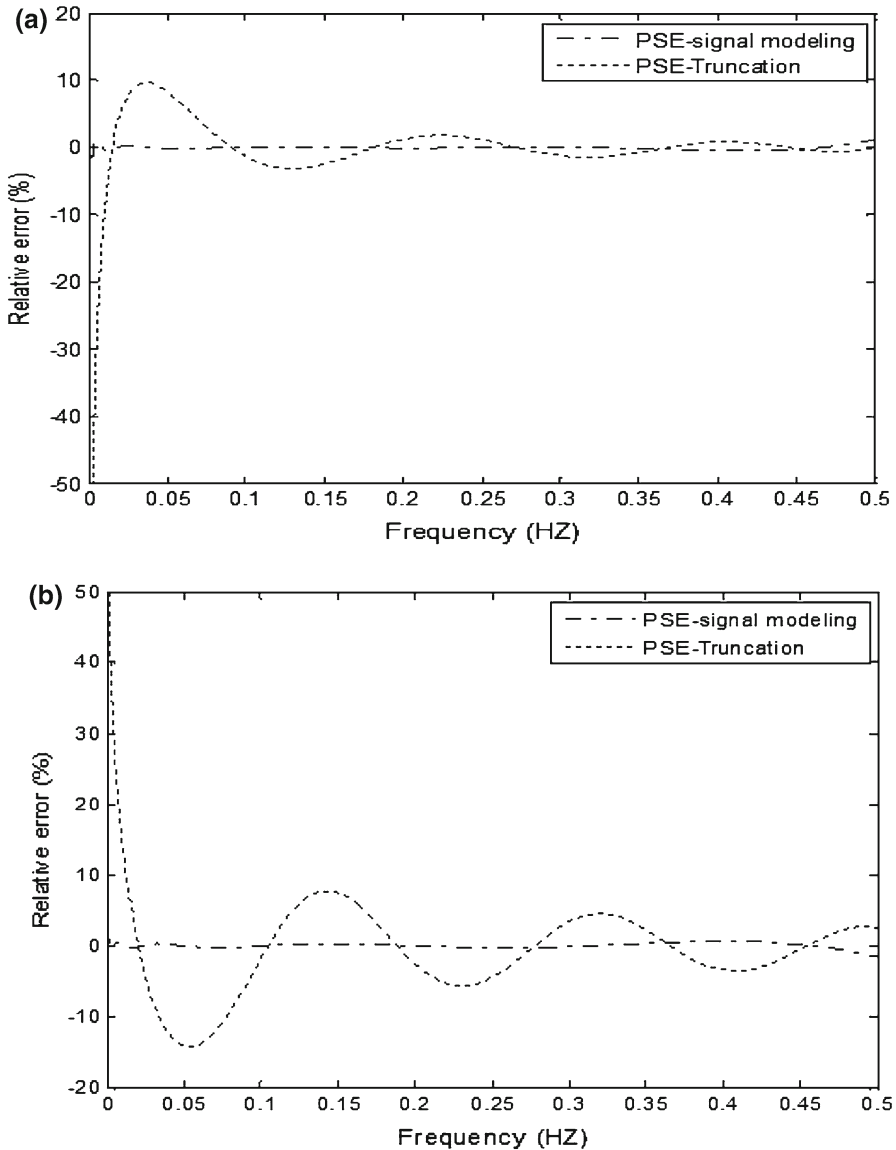
Fig. 12 Percent relative error, **a** $\alpha = 1/4$, **b** $\alpha = -1/4$

The magnitude and phase frequency responses of the obtained approximations are shown in Fig. 14 and compared to models obtained using PSE-truncation with $p = q = 40$. The checking of the pole-zero maps shows that the poles and zeros are complex when using PSE-truncation.

Figure 15 presents the percent relative error in magnitude. We can observe that PSE-signal modeling presents the smallest error. Also, we can deduce that increasing the truncation order (q and p) of numerator and denominator results in slight improvement in the quality of the magnitude approximation using PSE- truncation.
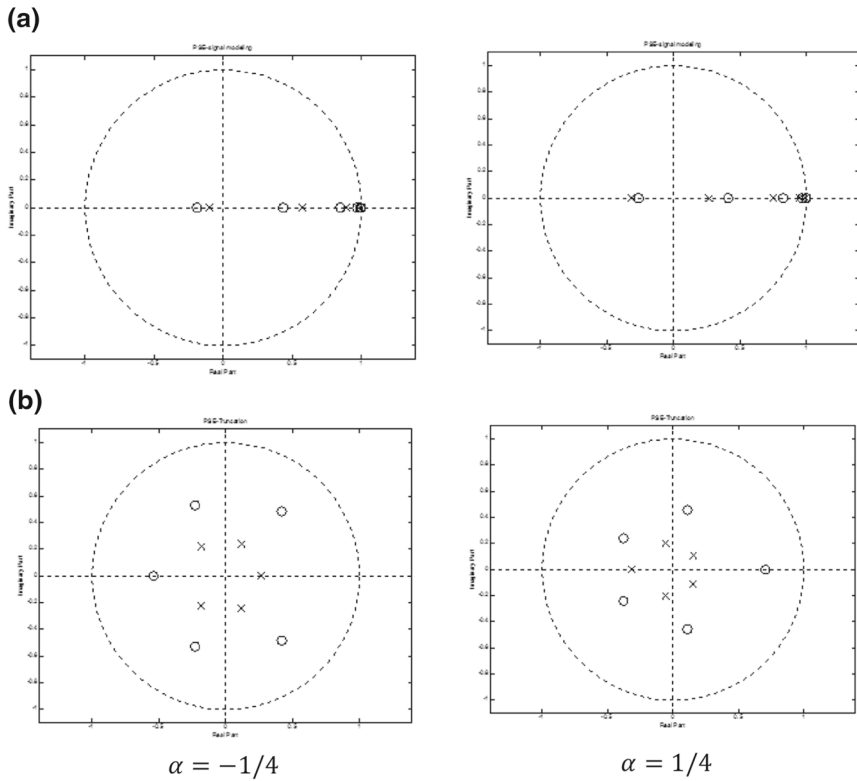
(a)

(b)

$$\alpha = -1/4 \qquad \alpha = 1/4$$

Fig. 13 Poles-zeros diagram, **a** PSE-signal modeling, **b** PSE-truncation

Table 4 Coefficients of the rational approximations based on Al-Alaoui's operator

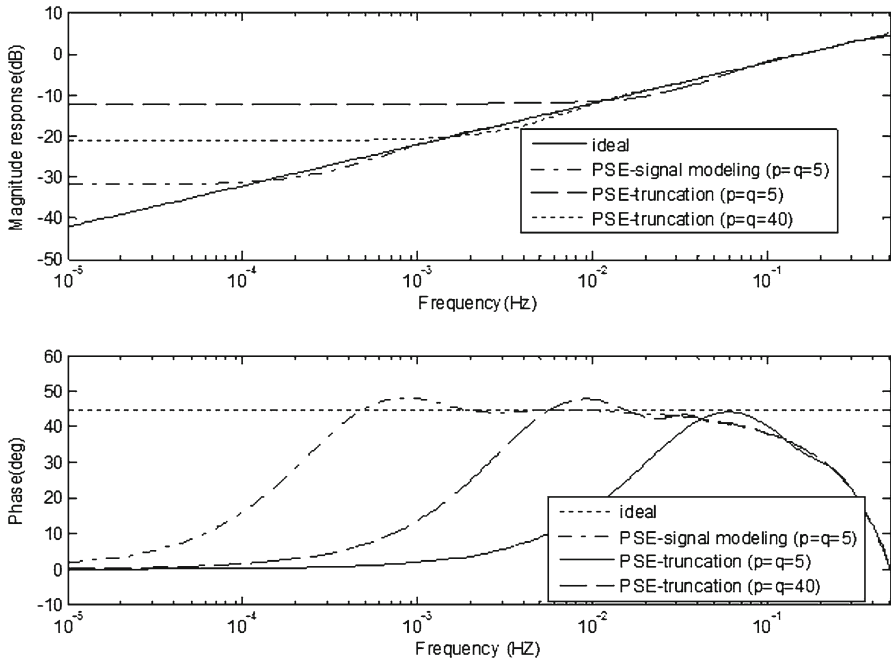|		PSE-signal Modeling	PSE-Truncation
B(z)	b_0	1.069044967644567	1.069044967649698
	b_1	−3.789489561781301	−0.534522483824849
	b_2	5.080791711801894	−0.133630620956212
	b_3	−3.129840761402043	−0.066815310478106
	b_4	0.831436092275494	−0.041759569048816
	b_5	−0.061940142505705	−0.029231698334171
A(z)	a_0	1.000000000000000	1.000000000000000
	a_1	−2.973314461443737	0.071428571428571
	a_2	3.135238561983327	−0.002551020408163
	a_3	−1.320541978722998	0.000182215743440
	a_4	0.140837398772762	−0.000016269262807
	a_5	0.017868591240445	0.000001626926281

Fig. 14 Magnitude and phase responses of s^α and the approximations obtained using PSE-signal modeling and PSE-truncation based on Al-Alaoui's operator
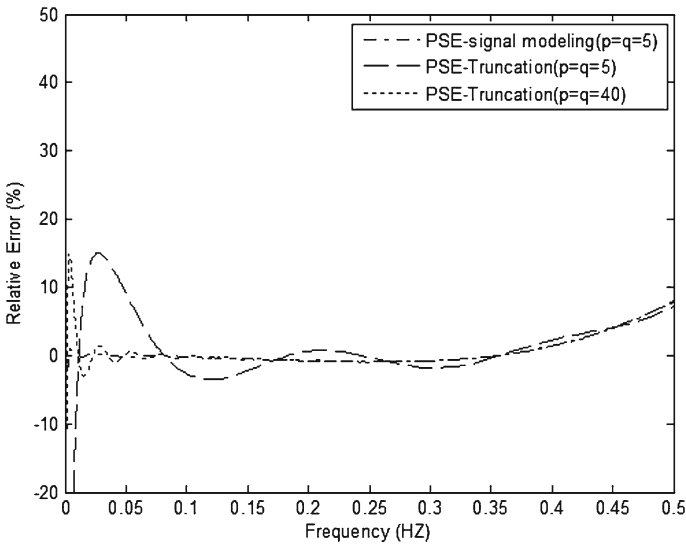

Fig. 15 Percent relative error for $\alpha = 0.5$

5 Conclusion

An improved digital rational approximation of s^α obtained via PSE-signal-modeling technique by using a new second-order s-to-z transform was presented and compared to recently used s-to-z transforms based models. Moreover, PSE-signal modeling has also been compared to PSE-truncation technique. The main advantages of the proposed approach are the following:

– The new second-order s-to-z transform has better magnitude response in almost over the full Nyquist band than the recently used first-order and higher order s-to-z transforms with the lower relative error in magnitude which is preferred for real-time application.
– The PSE-signal-modeling techniques (Prony, Shanks, Padé, and Steiglitz MC-Bride) of the fractional power of second-order operator (FPSOO) can be accomplished and lead to stable models .The drawback is that the approach requires more arithmetic operations to compute the FPSOO's impulse response as compared to the computation of the first-order operators' impulse response.
– In contrast to the recently used method based on PSE-truncation, PSE-signal-modeling approach does not lead to approximation with complex conjugate poles and zeros using first-order or second-order operators.
– Simulation results of magnitude response, phase response, and relative error show that the rational approximations obtained using PSE-signal modeling outperform those obtained using PSE-truncation based on first or second-order s-to-z transforms.

References

1. M.A. Al-Alaoui, Novel stable higher order s-to-z transforms. IEEE Trans. Circuits Syst. I Fundam. Theory Appl. **48**(11), 1326–1329 (2001)
2. M.A. Al-Alaoui, Novel class of digital integrators and differentiators. IET Signal Process **5**(2), 251–260 (2011)
3. M. Benmalek, A. Charef, Digital fractional order operators for R-wave detection in electrocardiogram signal. IET signal process **3**(5), 381–391 (2009)
4. T. Blaszczyk, M. Ciesielski, M. Klimek, J. Leszczynski, Numerical solution of fractional oscillator equation. Appl. Math. Comput. **218**(6), 2480–2488 (2011)
5. O. Cem, S. Melin, Y. Yavuz, An experimental performance evaluation for the suppression of vibrations of the second mode of a smart beam. in *Proceedings of Ankara International Aerospace Conference*, METU, Ankara, Turkey, 14–16 September, 2011, pp. 1–9
6. A. Charef, H.H. Sun, Y.Y. Tsao, B. Onaral, Fractal system as represented by singularity function. IEEE Trans. Autom. Control. **37**(9), 1465–1470 (1992)
7. Y.Q. Chen, K.L. Moore, Discretization schemes for fractional-order differentiators and integrators. IEEE Trans. Circuits Syst. I Fundam. Theory Appl. **49**(3), 363–367 (2002)
8. Y.Q. Chen, B.M. Vinagre, A new IIR-type digital fractional order differentiator. Signal Process **83**(11), 2359–2365 (2003)
9. Y. Ferdi, Computation of fractional order derivative and integral via power series expansion and signal modeling. Nonlinear Dyn. **46**(1–2), 1–15 (2006)
10. Y. Ferdi, Impulse invariance-based method for the computation of fractional integral of order $0 < \alpha < 1$. Comput. Electr. Eng. **35**(5), 722–729 (2009)

11. Y. Ferdi, Improved lowpass differentiator for physiological signal processing. in *Proceedings of IEEE 7th International Conference on Communication Systems Networks and Digital Signal Process. (CSNDSP)*, Newcastle upon Tyne, England, 21–23, July, 2010, pp. 747–750

12. Y. Ferdi, Fractional order calculus-based filters for biomedical signal processing. in *Proceedings of IEEE 1st Middle East Conference on Biomedical Engineering (MECBME)*, Sharjah, UAE, 21–24, February, 2011, pp. 73–76

13. Y. Ferdi, A. Taleb-Ahmed, M.R. Lakehal, Efficient generation of $1/f^\beta$ noise using signal modeling techniques. IEEE Trans. Circuits Syst. I **55**(6), 1704–1710 (2008)

14. M. Gupta, P. Varshney, G.S. Visweswaran, Digital fractional order differentiator and integrator models based on first and higher order operators. Int. J. Circ. Theor. Appl. (2010). doi:10.1002/cta.650

15. B.T. Krishna, Binary phase coded sequence generation using fractional order logistic equation. Circuits. Syst. Signal Process **31**(1), 401–411 (2012)

16. B.T. Krishna, K.V.V.S. Reddy, Design of fractional order digital differentiators and integrators using indirect discretization. Int. J. Circ. Theor. Appl. **11**(2), 143–151 (2008)

17. P. Kumar, O.P. Agrawal, An approximate method for numerical solution of fractional differential equations. Signal Process **86**, 2602–2610 (2006)

18. P. Lanusse, H. Benlaoukli, D. Nelson-Gruel, A. Oustaloup, Fractional-order control and interval analysis of SISO systems with time-delayed state. IET Cont. Theory Appl. **2**(1), 16–23 (2008)

19. F. Leulmi, Y. Ferdi, An improvement of the rational approximation of the fractional operator s^α. in *Proceedings of IEEE International Conference on Electronics, Communications and Photonics Conference (SIECPC)*, Riyadh, Saudi Arabia, 24–26, April, 2011, pp. 1–6

20. Y. Li, H. Tang, H. Chen, Fractional order derivative spectroscopy for resolving simulated overlapped Lorenzian peaks. Chemom. Intell. Lab. Syst. **107**(1), 83–89 (2011)

21. J. Lu, M. Xie, Use fractional calculus in iris localization. in *Proceedings of International Conference Communications, Circuits and Systems (ICCCAS)*, Fujian, China, 25–27, May, 2008, pp. 946–949

22. G. Maione, High-speed digital realizations of fractional operators in delta domain. IEEE Trans. Autom. Control **56**(3), 697–702 (2011)

23. B. Mathieu, P. Melchior, A. Oustaloup, C. Ceyral, Fractional differentiation for edge detection. Signal Process **83**(11), 2421–2432 (2003)

24. C.A. Monje, F. Ramos, V. Feliu, B.M. Vinagre, Tip position control of a lightweight flexible manipulator using a fractional order controller. IET Cont. Theory Appl. **1**(5), 1451–1460 (2007)

25. I. Petras, Fractional-order feedback control of DC motor. J. Electr. Eng. **60**(3), 117–128 (2009)

26. A.G. Radwan, K.N. Salama, Fractional-order RC and RL circuits. Circuits Syst. Signal Process **31**(6), 1901–1915 (2012)

27. A. Razminia, A.F. Dizaji, V.J. Majd, Solution existence for non-autonomous variable-order fractional differential equations. Math. Comput. Model. **55**, 1106–1117 (2012)

28. C.C. Tseng, Digital integrator design using Simpson rule and fractional delay filter. IEE Proc. Vis. Image Signal Process **153**(1), 79–85 (2006)

29. C.C. Tseng, Design of FIR and IIR fractional order Simpson digital integrators. Signal Process **87**(5), 1045–1057 (2007)

30. P. Varshney, G.S. Visweswaran, First and higher order operator based fractional order differentiator and integrator models. in *Proceedings of 2009 IEEE Region 10 Conference*, TENCON 2009, pp. 1–6

31. B.M. Vinagre, I. Podlubny, A. Hernandez, V. Feliu, Some approximations of fractional order operators used in control theory and applications. Fract. Calc. Appl. Anal. **3**(3), 231–248 (2000)

32. G.S. Visweswaran, P. Varshney, M. Gupta, New approach to realize fractional power in z-domain at low frequency. IEEE Trans. Circuits syst. II Express. Briefs **58**(3), 179–183 (2011)

33. R. Yadav, M. Gupta, Design of fractional order differentiators and integrators using indirect discretization scheme IICPE, New Delhi, India, January. in *Proceedings of IEEE Indian International Conference on Power Electronics* 2011